sustainability

MDPI

Article

Photocatalytic Degradation of Methylene Blue Using Zinc Oxide Nanorods Grown on Activated Carbon Fibers

Borhan Albiss [1,*] and Muna Abu-Dalo [2]

[1] Nanomaterials & Magnetic Measurements Laboratory, Physics Department, Jordan University of Science and Technology, Irbid 22110, Jordan
[2] Chemistry Department, Jordan University of Science and Technology, Irbid 22110, Jordan; maabudalo@just.edu.jo
* Correspondence: baalbiss@just.edu.jo

Abstract: In this work, the synthesis, characterization, and photocatalytic performance of zinc oxide/activated carbon fiber nanocomposites prepared by hydrothermal method were investigated. Zinc oxide nanoparticles (ZnO-NP) were deposited as seeds on porous activated carbon fiber (ACF) substrates. Then, zinc oxide nanorods (ZnO-NR) were successfully grown on the seeds and assembled on the fibers' surface in various patterns to form ZnO-NR/ACF nanocomposites. The nanocomposites were characterized by scanning electron microscopy (SEM), X-ray diffraction (XRD), Fourier transform infrared (FTIR) spectrometry, UV–vis diffuse reflectance spectra (DRS), and Brunauer–Emmett–Teller (BET) surface area analysis. SEM images showed that brush-like and flower-like ZnO-NR patterns were grown uniformly on the ACF surface with sizes depending on the ZnO-NP concentration, growth time, and temperature. The FTIR spectrum confirmed the presence of the major vibration bands, especially the absorption peaks representing the vibration modes of the COOH (C = O and C = C) functional group. Adsorption and photocatalytic activities of the synthesized catalytic adsorbents were compared using methylene blue (MB) as the model pollutant under UV irradiation. ZnO-NR/ACF nanocomposites showed excellent photocatalytic activity (~99% degradation of MB in 2 h) compared with that of bare ZnO-NR and ACF. Additionally, a recycling experiment demonstrated the stability of the catalyst; the catalytic degradation ratio of ZnO-NR/ACF reached more than 90% after five successive runs and possessed strong adsorption capacity and high photocatalytic ability. The enhanced photocatalytic activities may be related to the effects of the relatively high surface area, enhanced UV-light absorption, and decrease of charge carrier recombination resulting from the synergetic adsorption–photocatalytic degradation effect of ZnO and ACF.

Keywords: zinc oxides nanorods; activated carbon fibers; photocatalysis; methylene blue

Citation: Albiss, B.; Abu-Dalo, M. Photocatalytic Degradation of Methylene Blue Using Zinc Oxide Nanorods Grown on Activated Carbon Fibers. *Sustainability* **2021**, *13*, 4729. https://doi.org/10.3390/su13094729

Academic Editor: Petros Kokkinos

Received: 13 March 2021
Accepted: 20 April 2021
Published: 23 April 2021

1. Introduction

Metal oxide semiconductors have been widely studied as photocatalysts to remove organic pollutants from air and water [1–4]. The photocatalysis process takes place through the activation of the metal oxides by suitable photon energy that generates the active sites of electron-hole pairs, which induce the catalytic activities on the metal oxides' surfaces [5]. Among these metal oxides, TiO_2 is considered as the earliest, most common, and ideal material because of its good stability and quite simple preparation method [6–9].

Zinc oxide (ZnO) is a metal oxide with a relatively wide band gap of 3.37 eV and the exciton binding energy of 60 m eV has been extensively studied as a photocatalyst for the decomposition of many organic pollutants. Additionally, ZnO nanostructures are considered as prominent photocatalyst candidates to be used in photodegradation due to their low cost, nontoxicity, and efficiency in absorption across the solar spectrum compared to TiO_2 [10]. In several reports, ZnO nanostructures exhibited good photocatalytic activities for the removal of organic pollutants such as organic dyes [11].

In this regard, several experimental studies have been reported on the enhancement of the photocatalytic performance of ZnO by doping with several elements [12], hybridization [13], mixing heterostructures with other semiconductors [14], and in the form of ZnO-based nanocomposite materials [15–19]. However, ZnO nanostructures in powder form are quite difficult to recycle from aqueous solutions after activation and experience deactivation when the nanoparticles are agglomerated or lost in the catalytic solution due to their small size.

Many scientists have begun to focus on finding a practical solution to the immobilization of ZnO nanostructures on a suitable substrate with various porosities such as porous ceramics, zeolite, FTO glass, Teflon, PDMS, rGO, and carbonaceous materials [20–28]. Among the several studies cited above, carbon materials such as carbon nanotubes (CNTs), carbon fibers (CFs), carbon quantum dots (c-dots), reduced graphene oxide (rGO), and activated carbon fibers (ACFs) have been used as support substrates for ZnO nanostructures [22,23].

ACFs have been widely used to remove dyes and water pollutants due to their large specific surface area of (1000–3000 m^2/g), strong adsorption capacity, and highly porous medium with a complex structure composed mainly of the graphitic structure of carbon atoms [26–28]. Most of these studies reported that ACFs have a favorable and synergistic effect on photodegradation efficiency when used as a flexible substrate or mixed with ZnO nanostructures. ACF is considered as a promising, highly efficient adsorption carbon material that can contribute to the photocatalysis mechanism, both alone and in combination with various semiconductor materials [29,30]. Furthermore, introducing ACFs to photocatalytic nanocomposites can not only improve their visible light catalytic efficiency, and enhance their generated electron-hole recombination rate, but also optimize their photocatalytic stability and enhance the charge transfer of the photogenerated (electron-hole) pairs.

In the past few years, studies have reported on the photocatalytic activities of ZnO/ACF nanocomposites prepared with different morphologies using various methods such as electrospinning, sol-gel, and hydrothermal methods [31–34].

For example, Li et al. [32] and Mu et al. [33] have studied the immobilization of ZnO nanostructures on ACFs by hydrothermal method and reported an improved photocatalytic degradation of dyes with good catalyst recyclability. More recently, another study reported the assembly of ZnO nanorod (ZnO-NR) arrays on the ACFs by an integrated sol-gel and hydrothermal method [34]. The preliminary results showed excellent methylene blue (MB) degradation of 77.5%. The removal of MB from aqueous solutions is of great importance from an environmental point of view. Thus, MB is usually used as a prototype contaminant in photocatalytic processes [35].

Due to the synergistic effect between the strong visible light adsorption of the ACFs and UV-light photocatalytic activity of ZnO nanostructures, the photocatalytic degradation of MB is expected to demonstrate that ZnO/ACF nanocomposites exhibit enhanced photocatalytic activities under both UV and visible light irradiation. To the best of our knowledge, except for the few reported results reviewed above, there is no available systematic analysis of the photocatalytic activities of the hierarchical nanostructures of ZnO/ACF nanocomposites using MB as a model organic pollutant.

In this contribution, unique ZnO nanostructures were prepared using a facile, simple, low-temperature, and cost-effective hydrothermal method in a Teflon-lined stainless steel sealed autoclave reactor, through which the optimum preparation conditions were controlled to enhance the nanostructures' quality and reproducibility, promote uniform and self-assembly of ZnO on ACFs, and boost their crystalline structure photocatalytic and adsorption properties. The novelty of using this hydrothermal autoclave reactor, compared to the conventional hydrothermal processes used in the few reported studies, allows deposition of seed crystals and formation of crystalline phases that are unstable at certain temperatures and pressures. Additionally, nanomaterials that tend to vaporize can also be safely synthesized using the sealed reactor. Prepared samples were characterized

using XRD, SEM, FT-IR, UV-vis, and BET techniques and evaluated via the photocatalytic degradation of MB under UV irradiation.

2. Materials and Methods

2.1. Materials

The Kynol™ activated carbon fiber samples, ACF-1603-10 (ACF10), used in this study were obtained from American Technical Trading, Inc. (Pleasantville, NY, USA). This type of ACFs is obtained by carbonization and gasification of a phenolic resin precursor. The average fiber length was about 3 mm and average fiber diameter 10 µm, with specific area of 1000 m^2 g^{-1} as stated by the manufacturer. Methylene blue (basic blue 9, C.I. 52015; chemical formula, $C_{16}H_{18}N_3ClS$, Merck) was used without further purification. Hexamethylenetetramine, HMT [$(CH_2)_6N_4$, 99%], and zinc nitrate hexahydrate [(Zn $(NO_3)_2 \cdot 6H_2O$, 98%], zinc acetate dihydrate Zn $(CH_3COO)_2 \cdot 2H_2O$, ammonia dihydrate $NH_3.H_2O$, and potassium hydroxide (KOH) of analytical reagent grade were purchased from Sigma-Aldrich (St. Louis, MO, USA) and directly used without modification.

2.2. Synthesis of ZnO-NP, ZnO Seeds on ACF, and ZnO-NR on ACF Nanocomposites

Pure ZnO-NPs and ZnO-NR grown on ACF were synthesized by a chemical precipitation and hydrothermal method as follows.

Firstly, 0.5 M of zinc acetate dihydrate was dissolved in 50 mL of double distilled water in which ammonia dihydrate was dissolved in 50 mL solution and added dropwise. The mixture was stirred for 1 h to obtain pure ZnO-NP.

Secondly, the ZnO-NP/ACF nanocomposite was synthesized by adding 0.5 g of ACF to the mixture, then the final mixture was stirred at 75 °C for 4 h. The obtained nanocomposite was filtered, washed several times with double distilled water and ethanol, dried at 100 °C for 5 h, and annealed in a tube furnace at 400 °C for 2 h to obtain the ZnO-NP/ACF with a seed layer.

Thirdly, for the growth of the ZnO-NR on ZnO-NP/ACF nanocomposite, an aqueous solution containing equimolar concentrations (25 mM) of zinc nitrate hexahydrate and (HMT) was prepared in 100 mL deionized water. The solution was separately agitated in a magnetic stirrer at 1000 rpm for 30 min. Then, 0.5 g of ZnO-NP/ACF nanocomposite was added to the solution and the mixture was subjected to a hydrothermal process by putting it into a Teflon-lined stainless steel sealed autoclave reactor at 120 °C for 2 h in a muffle furnace. For enhancing the reactivity and homogeneity of the solution, a magnetic stirrer was used. Then, the autoclave was cooled to room temperature.

Finally, the obtained ZnO-NR/ACF nanocomposite was filtered, flushed with DI water until the pH of the final solution was 7.0, and dried in a vacuum oven at 100 °C for 5 h. The amount of ZnO-NR loadings was determined by the weight difference of ACFs before and after the hydrothermal process.

A schematic diagram of the major steps in nanocomposite synthesis is illustrated in Figure 1.

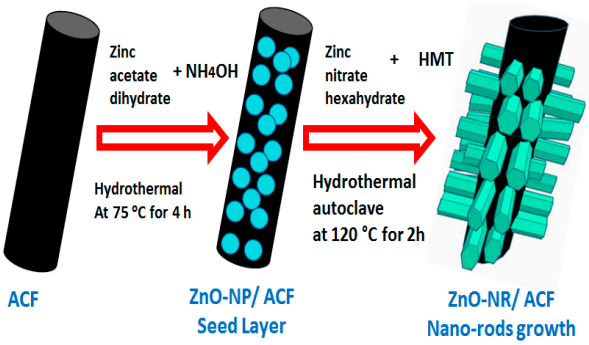

Figure 1. Schematic diagram of the zinc oxide nanorod/activated carbon fiber (ZnO-NR/ACF) synthesis process.

2.3. Characterization

The XRD diffractograms (with CuKα radiation and λ = 1.5406 Å) were performed using a Rigaku Ultima IV diffractometer. The UV-vis absorption spectra were recorded in the range 200–750 nm by a Varian/Carry 5000 spectrophotometer. The FTIR spectra were recorded in the wave number range of 4000–500 cm^{-1} using a BRUKER Alpha II spectrometer. The morphologies of samples were analyzed by FE-SEM (Quanta FEI 450). The N_2 adsorption–desorption was measured at 77 K (Micrometrics Tri Star II Plus).

The specific surface area and pore volumes of the ACF and ZnO-NR/ACF nanocomposite were determined by standard gas adsorption methods at 77 K. Using an adsorption model developed by Brunauer, Emmett, and Teller (BET) [36], the surface area (S_{BET}) was estimated. The total pore volume (V_P) was determined from the amount of N_2 adsorbed at the relative pressure (P/P_0) around 0.99. The desorption average pore diameter D_P was determined by the Barrett–Joyner–Halenda (BJH) method.

2.4. Photocatalytic Degradation of MB

The photocatalytic activities of the prepared photocatalysts (ZnO-NR and ZnO-NR/ACF) were evaluated by observing the degradation of methylene blue (MB) (a typical pollutant in the textile industry). MB stock solution was prepared by dissolving it in distilled water at 100 mg L^{-1} into a 250 mL beaker. Then, 10 mg of ZnO-NR, ACF, and ZnO-NR/ACF photocatalysts (each in a separate 10 mL bottle) were added to the MB solution at pH 6.7 $\pm$ 0.1. To ensure adsorption/desorption equilibrium of MB on these photocatalysts, the solutions were mixed using a magnetic stirrer in dark medium for 30 min and centrifuged at 3000 rpm for 5 min. The UV-vis absorption spectrum of the solution was measured in the range of 200–750 nm. Then, the mixture was exposed to a UV lamp (6 Watts, λ = 365 nm). The initial MB concentration was 50 mg L^{-1} and the temperature of the reaction solution was maintained at 30.0 $\pm$ 0.5 °C. Ten samples were taken with fixed time intervals of 10 and 20 min after UV radiation, and their absorption spectrum was recorded. The residual concentration of MB dye in the solution was measured at the major peak 664 nm using a UV-visible spectrophotometer. Blank (containing no dye) sample was used as a control and a calibration curve of absorbance versus concentration was constructed. Samples were collected at 10 min time intervals (up to 4 h) and centrifuged to remove the catalyst before analysis. The degradation efficiency of the MB was calculated by Equation (1).

$$\% \, Degradation = \frac{C_o - C_t}{C_o} \times 100 \quad (1)$$

where C_0 = initial MB concentration and C_t = MB concentration after time t.

Additionally, recycling experiments were conducted to explore the stability and photocatalytic ability of the ZnO-NR/ACF nanocomposite after five successive cycles. To test the recyclability of the ZnO-NR/ACF nanocomposite, it was removed from the irradiated solution and washed with DI water before starting the next cycle.

3. Results

3.1. XRD Analysis

The X-ray diffraction (XRD) patterns of ZnO-NR, ACF, and ZnO-NR/ACF nanocomposite are presented in Figure 2. The main peaks were indexed with Miller indices (h k l) which correspond to interplanar spacing of ZnO and ACF.

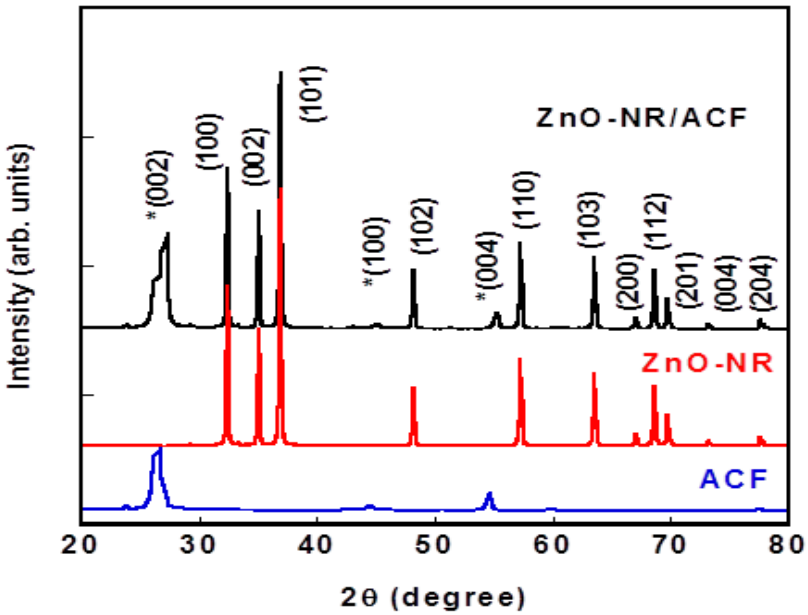

Figure 2. XRD diffraction pattern of ACF, ZnO-NR, and ZnO-NR/ACF. Peaks correspond to ACF are marked by (*).

Figure 2 shows all major peaks of the ZnO-NR/ACF nanocomposite and no obvious change could be identified in 2 θ values after the nanorods' growth on the ACF surface, indicating that ACF patterns were not disturbed. The indexed XRD reflections of ZnO-NR reveal a good agreement with all diffraction peaks assigned to the hexagonal wurtzite structure [JCPDS 36-1451] with lattice constants of a = 3.259 Å and b = 5.216 Å. The major reflections (002), (100), and (004) of ACF are present at both ACF and ZnO-NR/ACF patterns, which may indicate that ZnO-NR were self-assembled onto the ACF surfaces.

Moreover, all patterns showed a high degree of crystallinity and no traces of any impurity phases were observed in all XRD patterns. The sharp diffraction peaks indicate the good crystallinity of the prepared samples. The average crystallite sizes of the pure ZnO-NR and ZnO-NR in the ZnO-NR/ACF nanocomposite were estimated by Debye–Scherrer's formula [30]. Peaks with the highest intensities (100), (002), and (101) were used to calculate the average size of the ZnO-NRs. The average crystallite size calculated was 63.35 nm for pure ZnO-NR and 42.25 nm for ZnO-NR in the ZnO-NR/ACF nanocomposite. It is worth noting that the crystallite size is not necessarily the same as NR size depicted from the SEM images.

3.2. Scanning Electron Microscopy (SEM)

The SEM images of bare ACF and ZnO-NR/ACF nanocomposite are shown in Figure 3a–e, taken in different scanning areas and at selected magnifications. Figure 3a shows the SEM image of a felt of bare ACF without ZnO seeds or nanorods. The felt was composed of three smooth surface ACFs with diameters of approximately 8 to 12 µm and lengths ranging between 50 and 100 µm. Figure 3b shows that the ZnO-NRs were grown over the whole surface of the ACFs. The growth time was 2 h at temperature of 120 °C and under high pressure.

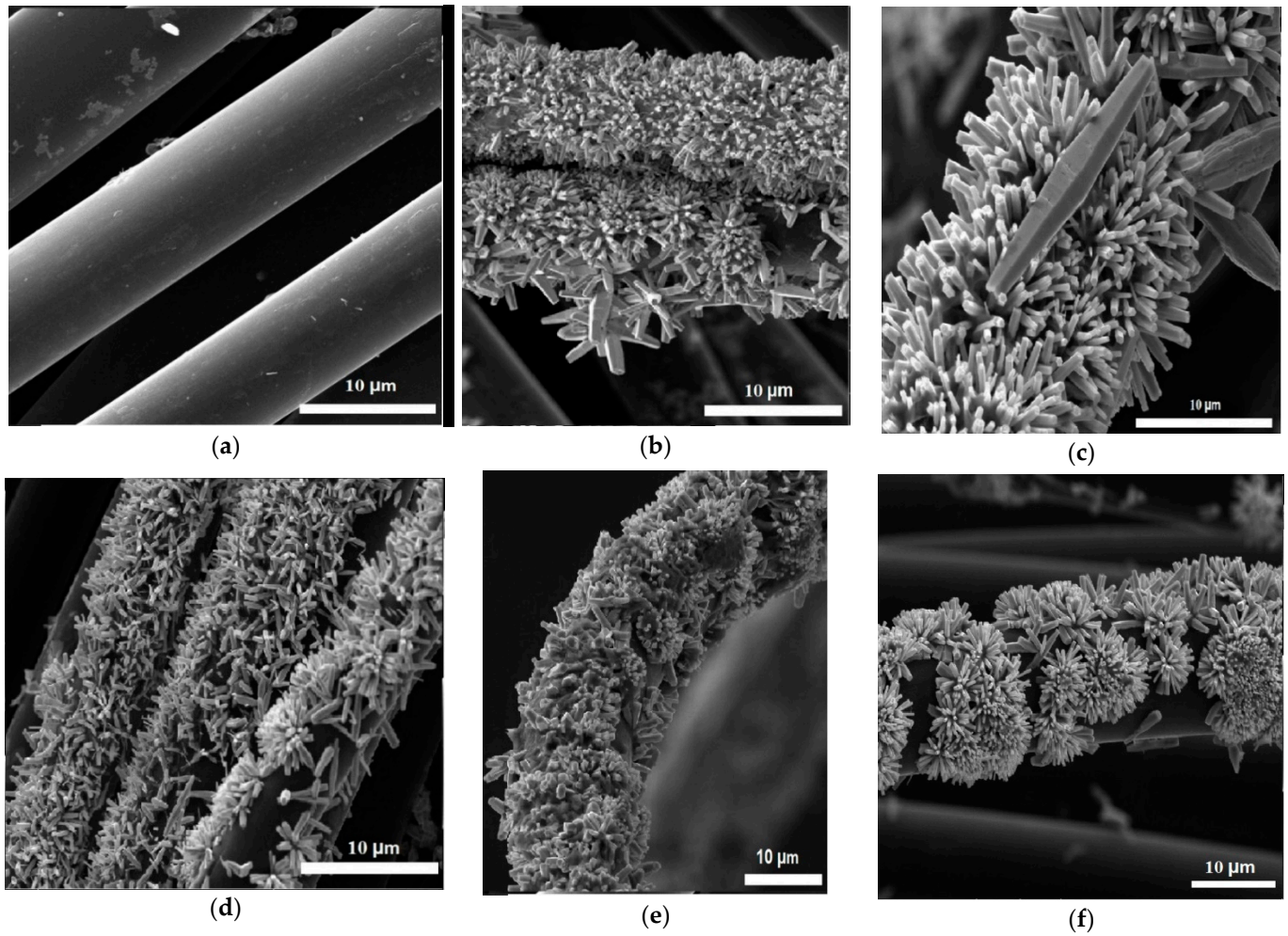

Figure 3. SEM images of bare ACF (**a**) and ZnO-NR loaded ACFs with different densities (**b**–**d**), ZnO-NR loaded on fiber after bending (**e**), and flower-like Zn-NR patterns (**f**).

Results revealed that the experimental conditions of the growth process, such as temperature, pressure, the pretreatment of the ACF substrates, and the concentration of the precursors have great influence on the ZnO-NRs' morphologies, and production of the optimum size and shape of the nanostructures. In addition, it could be clearly seen in Figure 3c that the ZnO-NRs were uniformly assembled on the ACFs' surface in all directions. In this process, fibers were floating freely in the growth solution during the NRs' growth so that all the surfaces of the ACF felt were exposed to Zn ions.

The uniformity of the ZnO-NPs seed layer is quite crucial during the growth process, because it introduces nuclei sites which let the ZnO-NR grow in dense patterns (Figure 3d). Furthermore, to ensure firm connection between the ZnO-NRs, ZnO-NPs, and the ACFs' surface, the ZnO-NR/ACF sample was washed several times with distilled water and agitated at a constant rate of 200 rpm for 2 h at room temperature. As shown in Figure 3e of the agitated sample, the ZnO-NRs were still well attached to the ACF surface even after fiber mechanical bending. The presence of flower-like and brush-like ZnO-NR patterns grown on some ACF fibers was also observed in the hierarchical nanostructures. This may be attributed to the formation of a few multi-particles and dense seed nucleation sites, which in turn provided better adsorption capacity for MB removal due to the relatively increased surface area and porosity of ZnO-NR/ACF compared to bare ACF and ZnO samples.

3.3. UV–Vis Absorption Spectrum of Bare ZnO-NRs and ZnO-NR/ACF

To explore the optical characteristics of the photocatalysts, the UV–vis absorption spectra of bare ZnO-NRs and ZnO/ACF were recorded in Figure 4a. It can be seen from the figure that the absorption edge of pure ZnO-NRs was about 380 nm. However, for ZnO-NR/ACF, the absorption edge was about 370 nm and exhibited a slight red shift compared with ZnO-NRs. Moreover, a considerable decrease in the absorbance was observed for the ZnO-NR/ACF in the whole spectrum range. This decrease in the absorbance of the nanocomposites following the growth of ZnO-NRs might have been due to obstruction of the light by the NRs' heterostructures.

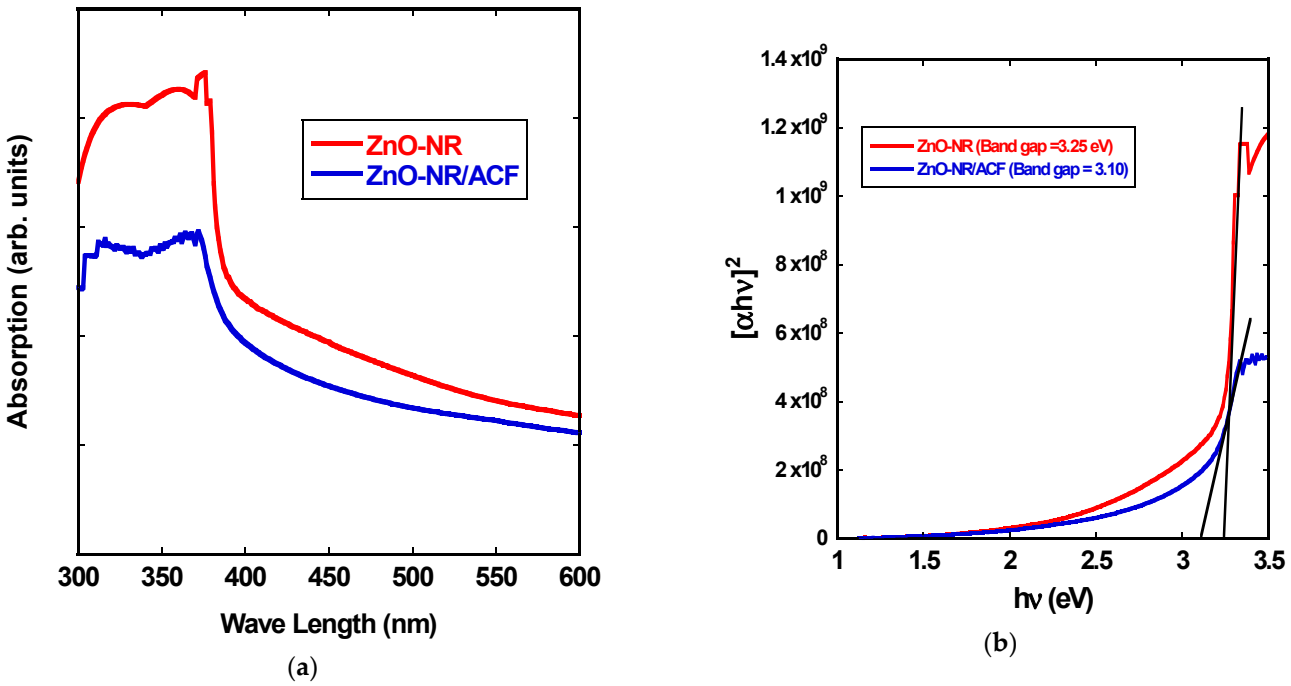

Figure 4. Diffuse reflectance spectra (DRS)-UV–vis spectra (**a**) and Tauc plots (**b**) for ZnO-NR and ZnO-NR/ACF.

DRS spectra and Tauc plots were analyzed to investigate the effect of ACFs' support on the band energy of the ZnO-NR. A Tauc equation was used to calculate the energy gap (E_g) of the samples [37]:

$$(\alpha h\nu)^{1/n} = A\,(h\nu - Eg)$$

where h, ν, α, and Eg are Planck's constant, frequency, absorption coefficient, and band gap energy, respectively. A is a constant, and $n = 1/2$ for directly allowed transitions. Figure 4b illustrates that plotting $(\alpha h\nu)^2$ versus photon energy (hν) reveals a linear region and the straight-line extrapolations to zero absorption represent (Eg) for bare ZnO-NR (Eg = 3.25 eV) and ZnO-NR/ACF (Eg = 3.10 eV). The reason of such difference in the optical Eg for different morphologies is related to the variation of the stoichiometry, size of the ZnO nanostructures, and the concentration of point defects. Furthermore, the decrease in the energy gap of ZnO-NR/ACF may be attributed to the change of energy level after loading of Zn-NRs on the ACF surface. This slight reduction of the band gap (about 2%) facilitated surface functionalization for the formation of hydroxyl radical (HO·).

3.4. FT-IR Analysis

To evaluate the surface chemistry of the synthesized nanocomposites, FTIR analysis was carried out. Figure 5 depicts the FT-IR spectra of the ZnO-NR, ACF, and ZnO-NR/ACF in the wave number range of 4000–500 cm^{-1}. The absorption peak at 3439 cm^{-1} may be assigned to the bending vibrations of the adsorbed water molecules and stretching vibrations of OH groups. The absorption peaks in the range of 1620–1730 cm^{-1} correspond

to C = O stretching. The carbonyl signal can be attributed to carboxylic acids, ketones, aldehydes, or esters. The C–H groups' stretching vibration peaks are at about 2840–2940 cm^{-1}, while the peak at 1038 cm^{-1} corresponds to the C-O stretching. This peak became more prominent for ZnO-NR/ACF due to the bonding between O atoms from ZnO with C on the ACF surface [29]. Moreover, the peaks at about 500–750 cm^{-1} (which appeared in ZnO-NR/ACF and ZnO-NR samples and are absent in the bare ACF spectrum) are related to the stretching mode of the Zn–O bond [33,38]. These FTIR spectra indicated a successful attachment between ZnO and ACFs. Similar results were observed by others [32,33,39].

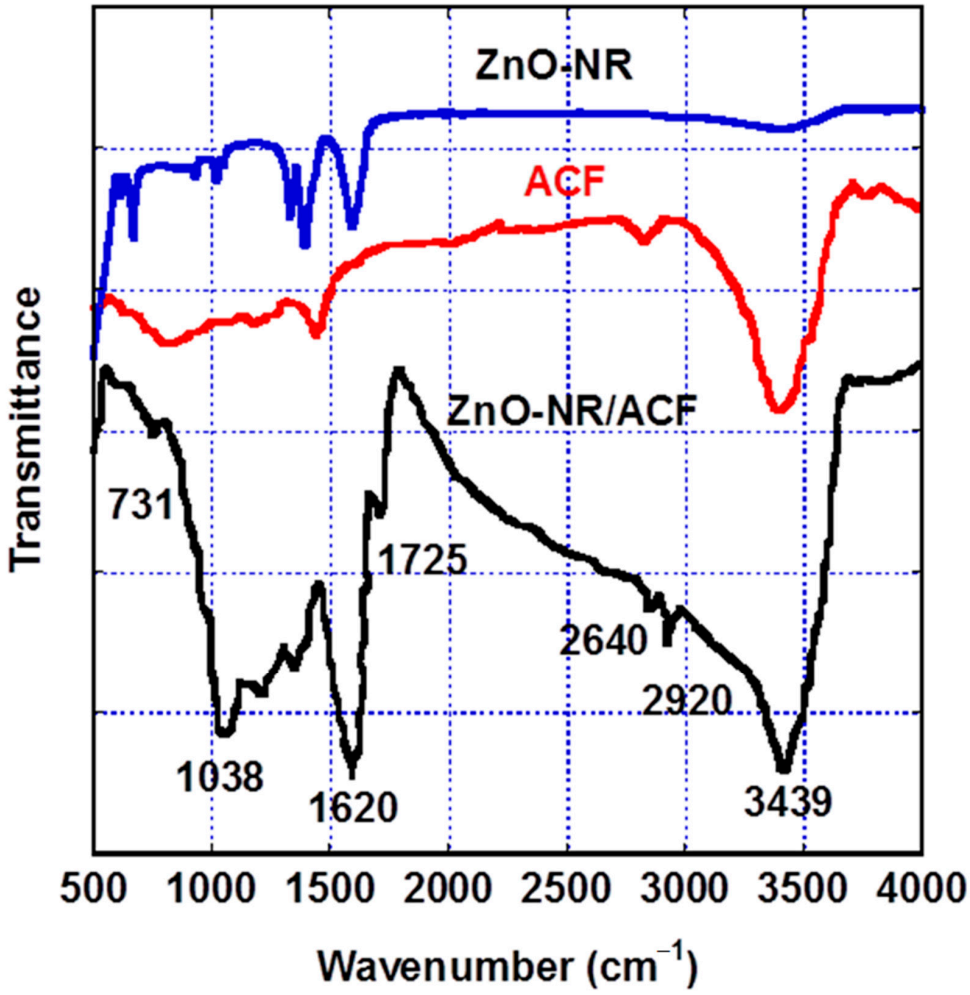

Figure 5. FTIR spectra for ZnO-NR, ACF, and ZnO-NR/ACF samples. Wavenumbers of vibration bands of the main absorption peaks were indexed.

3.5. BET Analysis

The surface area analysis using the BET method was employed to compare the surface properties of ACF and ZnO-NR/ACF nanocomposite. When zinc oxide nanorods (ZnO-NR) were grown on the seeds and assembled on the ACF surface, ZnO-NR/ACF realized a significant increase in specific surface area from 981 to 1050 m^2/g. Additionally, there was a decrease observed of total pore volume and pore diameter from 0.95 cm^3/g and 3.75 nm for ACF to 0.81 cm^3/g and 2.53 nm for ZnO-NR/ACF, respectively (Table 1).

Table 1. Textural properties of ACF and ZnO-NR/ACF.

Sample	S_{BET} (m^2/g)	V_p (cm^3/g) *	D_p (nm)
ZnO-NR	27 ± 0.5	0.15	4.31
ACF	981 ± 0.5	0.95	3.75
ZnO-NR/ACF	1050 ± 0.5	0.81	2.53

* Obtained from the volume of N_2 adsorbed at $P/P_0 = 0.98$.

The results indicated that the surface area and pore properties of ACF and ZnO-NR/ACF are larger than those of MB adsorbent or other adsorbents; i.e., the molecular size of the MB dye is 1.7 × 0.76 × 0.33 nm [40], which is less than the average pore diameter of ACF (3.75 nm) and ZnO-NR/ACF (2.53 nm), indicating that the MB dye molecules can easily enter the inner space of ACF and the photocatalyst nanocomposite and then disperse. Analogous effects were observed where commercial activated carbon fiber (ACF) was used for adsorption of methyl orange (MO) [41].

3.6. Photocatalytic Activity

In order to optimize the experimental conditions for the best photocatalytic performance of the nanocomposites, a systematic study was performed to find the optimum ZnO-NR, ACF, and MB concentrations for samples with excellent performance. Experiments with various pH media (acidic, neutral, and basic) were also conducted (see Table 2). The presented results revealed that the optimum results were obtained with samples of 20% wt. ZnO-NR load, pH of 7, and 50 mg/L MB concentrations at a degradation time of 120 min. The photocatalytic activities of the optimized samples were evaluated by observing the degradation of MB in the presence of ACF, ZnO-NR, and ZnO-NR/ACF under UV-light irradiation (Figure 6a). During the first 30 min (dark adsorption test), all samples showed a stable adsorption–desorption equilibrium in MB solution. For comparison, we also studied the photocatalytic degradation of MB by direct photolysis, i.e., without using a catalyst under identical experimental conditions. A negligible degradation of MB (~2%) over 2 h was observed, indicating that the properties of methylene blue are more stable. ACFs showed ~50% of the MB dye reduction during the first 2 h of UV-light irradiation, likely due to the high surface area, porosity, and superior adsorption properties, as indicated in the BET results. The photocatalytic results also showed that about 86% of MB was removed by ZnO-NRs, whereas a higher MB reduction of 99% was observed for ZnO-NR/ACF nanocomposite. The enhanced photocatalytic performance in the case of the ZnO-NR/ACF nanocomposite is attributed to the synergistic effects between ZnO nanorods and activated carbon fibers (ACFs), which can decrease the rate of recombination of electron-hole pairs caused by the trapping of excited electrons from the conduction band of ZnO-NR [26,27,41–47].

In addition to MB molecules' adsorption by highly porous activated carbon (AC) or ACFs [48–51], it has been reported that their photocatalytic activity relies on the particle size, phase structure, adsorption capability, and e−/h+ recombination rate [52]. It is suggested that the adsorption and degradation processes take place simultaneously in the ZnO-NR/ACFs. In addition, their unique microstructural features may play a role in enhancing electron transportation and reducing the recombination of electron-hole (e−/h+) pairs [53,54].

Table 2. Optimization of experimental conditions for better adsorption and photocatalytic degradation of methylene blue (MB).

Sample (at 500 mg/L)	MB Concentration (mg/L)	pH	MB Photodegredation (%) at 120 min	ZnO-NR Load (% wt.)
ZnO-NR	25	4	82%	100%
	50	7	86%	
	100	12	77%	
ACF	25	4	56%	0
	50	7	58%	
	100	12	61%	
ZnO-NR/ACF	25	4	88%	10%
		7	87%	
		12	88%	
	50	4	81%	20%
		7	99%	
		12	81%	
	100	4	82%	40%
		7	92%	
		12	78%	

The photodegradation reactions for MB (Figure 6b) exhibit pseudo-first-order kinetics and are estimated using Equation (2):

$$Ln\left(\frac{C}{Co}\right) = -k\,t \quad (2)$$

where (k) is the rate constant and (t) is the UV irradiation time.

The degradation of MB by the ZnO-NR/ACF photocatalyst exhibited quite fast kinetics with a rate constant of k = 0.042 min^{-1}, which is more than 2.5 times the rate constant of the ZnO-NR photocatalyst (k = 0.017 min^{-1}) and 7 times the rate constant of bare ACF (k = 0.006 min^{-1}). The photodegradation kinetics show that the photocatalytic activity of ZnO-NR/ACF was considerably higher, with faster kinetics, compared to that of ZnO-NR and ACF. This result can be explained in terms of the formation of the unique assembly of the microstructure with a large surface area of ZnO-NR/ACF compared to bare ACF. These findings are in good agreement with the obtained SEM and XRD results.

The unique microstructural features and high surface areas of ZnO-NR/ACF demonstrated great potential for photocatalytic application as illustrated in the photocatalytic degradation of methylene blue (MB) in solution (as seen in the UV–vis spectra in Figure 6c). In addition to their excellent photocatalytic degradation properties, Figure 6d demonstrated robust recyclability for ZnO-NR/ACF nanocomposites; after five times of their reuse, no significant changes were observed. The decrease in photocatalytic performance of ZnO-NR/ACFs was less than 5% in the presence of 50 mg L^{-1} of MB, after t = 750 min and at 500 mg of the photocatalyst under UV irradiation.

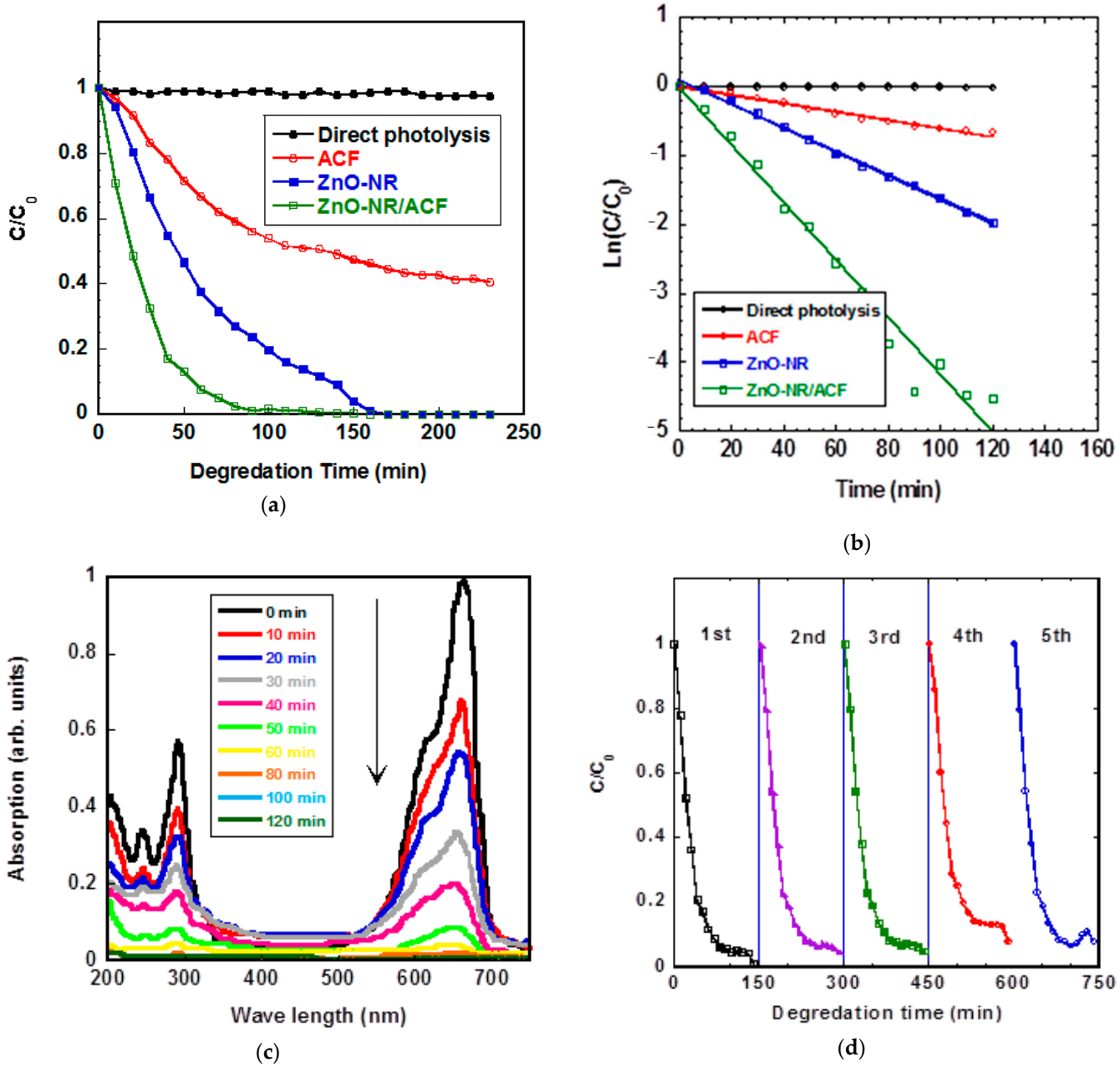

Figure 6. (**a**) Comparison of photodegradation of MB using different photocatalysts (Zn-NR, ACF, and ZnO-NR/ACF) under UV-light irradiation. (**b**) Kinetics of MB photocatalytic degradation (ln (C/C_0)) versus irradiation time. (**c**) UV–vis absorption spectra of aqueous MB during the decomposition reaction under UV-visible light irradiation in the presence of ZnO-NR/ACF nanocomposite. (**d**) Reusability results of the five cycles of MB degradation experiments at 50 mg L^{-1} dye concentrations under UV-light irradiation using ZnO-NR/ACF nanocomposite.

3.7. Photocatalytic Degredation Mechanism of MB under UV-Light Irradiation

Degradation of MB in the aqueous solution under UV-light irradiation and photocatalytic mechanism of the ZnO/ACF nanocomposites have been investigated by few research studies [27,28,34]. However, the proposed mechanism for ZnO-NR/ACF used in this study is illustrated in Figure 7.

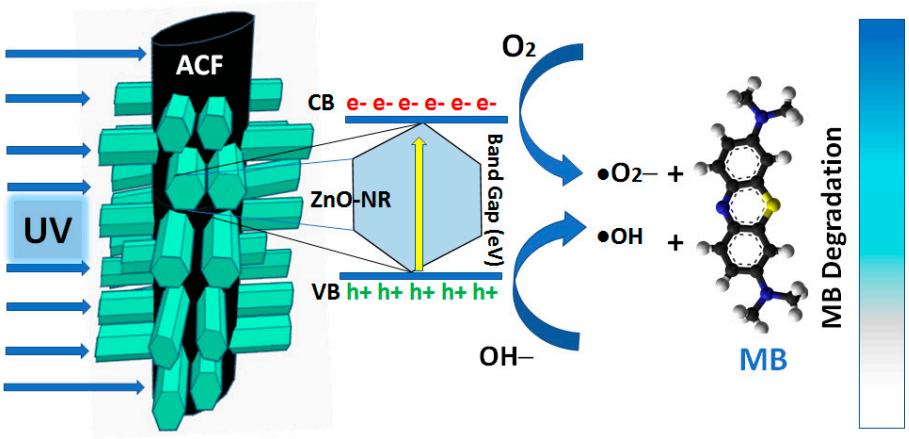

Figure 7. Photocatalytic degradation mechanism of MB under UV-light irradiation using ZnO-NR/ACF as a photocatalyst.

The proposed mechanism is summarized as follows:

- ZnO-NRs irradiated under UV light allow excited electrons to be transferred from the valence band (VB) to conduction band (CB). As a result, holes (h+) and electron (e−) will be generated in the VB and CB, respectively. The band gap is defined as the energy difference between the VB and CB.
- Electrons in the CB of ZnO-NRs are easily transferred to CB of ACFs due to the high electric conductivity of carbon. This leads to the excitation of MB molecules adsorbed onto the ZnO-NR/ACF surface.
- Photoelectrons resulting from the reaction react with O_2 molecules in the solution forming ($O_2 \cdot -$), while holes (h+) react with H_2O to form (·OH) that follows chain reactions.
- The ($O_2 \cdot -$) and (·OH) radicals react with MB molecules to convert the organic pollutants or into nontoxic forms or completely decompose them to CO_2 and H_2O. Both of the photodegradation processes are responsible for the degradation of the MB.

4. Conclusions

In summary, ZnO-NRs were grown successfully on the surface of a Zn-NP-seeded activated carbon fiber (ZnO-NP/ACF) via a sequential sol-gel and hydrothermal synthesis method in a growth solution of hexamethylenetetramine mixed with zinc nitrate hexahydrate solution at 95 °C. The structural and optical properties, morphology, and photocatalytic activities of the resultant ZnO-NR/ACF with optimum hydrothermal times and initial concentrations were investigated. The ZnO-NR/ACF sample with optimum concentration showed higher photocatalytic activity and MB degradation (99% in 2 h) compared to the pristine ACF and ZnO-NR samples, which may be attributed to the increase of effective charge transfer from ZnO-NRs to ACFs due to the electric conductivity of ACFs, increase in the nanocomposite surface area, and multidirectional light-capture by the ZnO-NR flower-like and brush-like patterns. Moreover, ZnO-NR/ACF nanocomposite can be used repeatedly with almost no change in photocatalytic activity after five cycles. Such nanocomposite with improved properties shows great potential to be used as an effective photocatalyst adsorbent and opens new horizons for its practical application in removing organic pollutants from aqueous solutions.

Author Contributions: B.A. and M.A.-D. shared the experimentation data analysis and manuscript preparation and editing. Both authors have read and agreed to the published version of the manuscript.

Funding: This research was funded by the deanship of research at Jordan University of Science and Technology, Jordan, grant number 2016-150.

Institutional Review Board Statement: Not applicable.

Informed Consent Statement: Not applicable.

Data Availability Statement: Data of this research is available upon request via corresponding author.

Acknowledgments: The authors would like to acknowledge the deanship of research at Jordan University of Science and Technology, Jordan for funding support, with thanks to Saja Alrousan and Sezar Alzoubi for their technical help in the nanomaterial's lab.

Conflicts of Interest: The authors declare no conflict of interest.

References

1. Nagpal, M.; Kakkar, R. Use of metal oxides for the adsorptive removal of toxic organic pollutants. *Sep. Purif. Technol.* **2019**, *211*, 522–539. [CrossRef]
2. Wawrzkiewicz, M.; Wiśniewska, M.; Wołowicz, A.; Gun'ko, V.M.; Zarko, V.I. Mixed silica-alumina oxide as sorbent for dyes and metal ions removal from aqueous solutions and wastewaters. *Microporous Mesoporous Mater.* **2017**, *250*, 128–147. [CrossRef]
3. Danish, M.S.S.; Bhattacharya, A.; Stepanova, D.; Mikhaylov, A.; Grilli, M.L.; Khosravy, M.; Senjyu, T. A Systematic Review of Metal Oxide Applications for Energy and Environmental Sustainability. *Metals* **2020**, *10*, 1604. [CrossRef]
4. Huang, Y.; Su, W.; Wang, R.; Zhao, T. Removal of typical industrial gaseous pollutants: From carbon, zeolite, and metal-organic frameworks to molecularly imprinted adsorbents. *Aerosol Air Qual. Res.* **2019**, *19*, 2130–2150. [CrossRef]
5. Lee, K.M.; Lai, C.W.; Ngai, K.S.; Juan, J.C. Recent developments of zinc oxide based photocatalyst in water treatment technology: A review. *Water Res.* **2016**, *88*, 428–448. [CrossRef]
6. Hashimoto, K.; Irie, H.; Fujishima, A. TiO_2 photocatalysis: A historical overview and future prospects. *Jpn. J. Appl. Phys.* **2005**, *44*, 8269–8285. [CrossRef]
7. Dastan, D.; Panahi, S.L.; Chaure, N.B. Characterization of titania thin films grown by dip-coating technique. *J. Mater. Sci. Mater. Electron.* **2016**, *27*, 12291–12296. [CrossRef]
8. Dastan, D.; Panahi, S.L.; Yengantiwar, A.P.; Banpurkar, A.G. Morphological and electrical studies of titania powder and films grown by aqueous solution method. *Adv. Sci. Lett.* **2016**, *22*, 950–953. [CrossRef]
9. Dastan, D. Effect of preparation methods on the properties of titania nanoparticles: Solvothermal versus sol-gel. *Appl. Phys. A* **2017**, *1–13*, 123–699. [CrossRef]
10. Azmina, M.S.; Nor, R.M.; Rafaie, H.A.; Razak, N.S.A.; Sani, S.F.A.; Osman, Z. Enhanced photocatalytic activity of ZnO nanoparticles grown on porous silica microparticles. *Appl. Nanosci.* **2017**, *7*, 885–892. [CrossRef]
11. Hariharan, C. Photocatalytic degradation of organic contaminants in water by ZnO nanoparticles: Revisited. *Appl. Catal. A Gen.* **2006**, *304*, 55–61. [CrossRef]
12. Vaiano, V.; Matarangolo, M.; Murcia, J.J.; Rojas, H.; Navío, J.A.; Hidalgo, M.C. Enhanced photocatalytic removal of phenol from aqueous solutions using ZnO modified with Ag. *Appl. Catal. B Environ.* **2018**, *225*, 197–206. [CrossRef]
13. Wang, Z.; Liu, S.; Zhang, J.; Yan, J.; Zhao, Y.; Mahoney, C.; Ferebee, R.; Luo, D.; Pietrasik, J.; Bockstaller, M.R.; et al. Photocatalytic active mesoporous carbon/ZnO hybrid materials from block copolymer tethered ZnO nanocrystals. *Langmuir* **2017**, *33*, 12276–12284. [CrossRef] [PubMed]
14. Zhou, G.; Xu, X.; Ding, T.; Feng, B.; Bao, Z.; Hu, J. Well–steered charge–carrier transfer in 3D branched CuXo/ZnO@ Au heterostructures for efficient photocatalytic hydrogen evolution. *ACS Appl. Mater. Interfaces* **2015**, *7*, 26819–26827. [CrossRef] [PubMed]
15. Ong, W.J.; Voon, S.Y.; Tan, L.L.; Goh, B.T.; Yong, S.T.; Chai, S.P. Enhanced daylight-induced photocatalytic activity of solvent exfoliated graphene (SEG)/ZnO hybrid nanocomposites toward degradation of reactive black 5. *Ind. Eng. Chem. Res.* **2014**, *53*, 17333–17344. [CrossRef]
16. Qamar, M.A.; Shahid, S.; Javed, M.; Sher, M.; Iqbal, S.; Bahadur, A.; Li, D. Fabricated novel g-C3N4/Mn doped ZnO nanocomposite as highly active photocatalyst for the disinfection of pathogens and degradation of the organic pollutants from wastewater under sunlight radiations. *Colloids Surf. A Physicochem. Eng. Asp.* **2021**, *611*, 125863. [CrossRef]
17. Murali, A.; Sarswat, P.K.; Free, M.L. Adsorption-coupled reduction mechanism in ZnO-Functionalized MWCNTs nanocomposite for Cr (VI) removal and improved anti-photocorrosion for photocatalytic reduction. *J. Alloy Compd.* **2020**, *843*, 155835. [CrossRef]
18. Kumaresan, N.; Sinthiya, M.M.A.; Ramamurthi, K.; Babu, R.R.; Sethuraman, K. Visible light driven photocatalytic activity of ZnO/CuO nanocomposites coupled with rGO heterostructures synthesized by solid-state method for RhB dye degradation. *Arab. J. Chem.* **2020**, *13*, 3910–3928. [CrossRef]
19. You, J.; Xiang, Y.; Ge, Y.; He, Y.; Song, G. Synthesis of ternary rGO–ZnO–Fe_3O_4 nanocomposites and their application for visible light photocatalytic degradation of dyes. *Clean Technol. Environ. Policy* **2017**, *19*, 2161–2169. [CrossRef]
20. Bagnara, M.; Farias, J.; Lansarin, M.A. Obtaining ZnO Immobilized Over Different Substrates by Hydrothermal Treatment for Photocatalysis Application. *Química Nova* **2016**, *39*, 286–291. [CrossRef]
21. Wang, L.; Liu, G.; Zou, L.; Xue, D. Phase evolution from rod-like ZnO to plate-like zinc hydroxysulfate during electrochemical deposition. *J. Alloy Compd.* **2010**, *493*, 471–475. [CrossRef]

22. Sinha, R.; Roy, N.; Mandal, T.K. Growth of Carbon Dot-Decorated ZnO Nanorods on a Graphite-Coated Paper Substrate to Fabricate a Flexible and Self-Powered Schottky Diode for UV Detection. *ACS Appl. Mater. Interfaces* **2020**, *12*, 33428–33438. [CrossRef]
23. Ebrahimi, S.; Bordbar-Khiabani, A.; Yarmand, B. Immobilization of rGO/ZnO hybrid composites on the Zn substrate for enhanced photocatalytic activity and corrosion stability. *J. Alloy Compd.* **2020**, *845*, 156219. [CrossRef]
24. Farhat, O.F.; Halim, M.M.; Abdullah, M.J.; Ali, M.K.M.; Ahmed, N.M.; Allam, N.K. Growth of vertically aligned ZnO nanorods on Teflon as a novel substrate for low-power flexible light sensors. *Appl. Phys. A* **2015**, *119*, 1197–1201. [CrossRef]
25. Albiss, B.A.; AL-Akhras, M.A.; Obaidat, I. Ultraviolet photodetector based on ZnO nanorods grown on a flexible PDMS substrate. *Int. J. Environ. Anal. Chem.* **2015**, *95*, 339–348. [CrossRef]
26. Thi, V.H.T.; Lee, B.K. Great improvement on tetracycline removal using ZnO rod-activated carbon fiber composite prepared with a facile microwave method. *J. Hazard. Mater.* **2017**, *324*, 329–339.
27. Chen, G.; Wang, Y.; Shen, Q.; Song, Y.; Chen, G.; Yang, H. Synthesis and enhanced photocatalytic activity of 3D flowerlike ZnO microstructures on activated carbon fiber. *Mater. Lett.* **2014**, *123*, 145–148. [CrossRef]
28. Nasrollahzadeh, M.S.; Hadavifar, M.; Ghasemi, S.S.; Chamjangali, M.A. Synthesis of ZnO nanostructure using activated carbon for photocatalytic degradation of methyl orange from aqueous solutions. *Appl. Water Sci.* **2018**, *8*, 1–12. [CrossRef]
29. Pant, B.; Barakat, N.A.; Pant, H.R.; Park, M.; Saud, P.S.; Kim, J.W.; Kim, H.Y. Synthesis and photocatalytic activities of CdS/TiO_2 nanoparticles supported on carbon nanofibers for highly efficient adsorption and simultaneous decomposition of organic dyes. *J. Colloid Interface Sci.* **2014**, *434*, 159–166. [CrossRef] [PubMed]
30. Ge, J.; Zhang, Y.; Park, S.J. Recent advances in carbonaceous photocatalysts with enhanced photocatalytic performances: A mini review. *Materials* **2019**, *12*, 1916. [CrossRef] [PubMed]
31. Pant, B.; Park, M.; Kim, H.Y.; Park, S.J. Ag-ZnO photocatalyst anchored on carbon nanofibers: Synthesis, characterization, and photocatalytic activities. *Synth. Met.* **2016**, *220*, 533–537. [CrossRef]
32. Li, P.; Liu, F.; Liu, Y.; Xue, R.; Fan, X. Preparation and photocatalytic activity of visible light-responsive zinc oxide/activated carbon fiber composites. *J. Dispers. Sci. Technol.* **2020**, 1–12. [CrossRef]
33. Mu, J.; Shao, C.; Guo, Z.; Zhang, Z.; Zhang, M.; Zhang, P.; Chen, B.; Liu, Y. High photocatalytic activity of ZnO− carbon nanofiber heteroarchitectures. *ACS Appl. Mater. Interfaces* **2011**, *3*, 590–596. [CrossRef] [PubMed]
34. Luo, S.; Liu, C.; Zhou, S.; Li, W.; Ma, C.; Liu, S.; Yin, W.; Heeres, H.J.; Zheng, W.; Seshan, K.; et al. ZnO nanorod arrays assembled on activated carbon fibers for photocatalytic degradation: Characteristics and synergistic effects. *Chemosphere* **2020**, *261*, 127731. [CrossRef]
35. German Standard No. 52980. Photocatalytic Activity of Surfaces-Determination of Photocatalytic Activity by Degradation of Methylene Blue. *Ger. Inst. Stand. (Deutsches Inst. für Normung)* **2008**, *10*, 1–14.
36. Brunauer, S.; Emmett, P.H.; Teller, E. Adsorption of gases in multimolecular layers. *J. Am. Chem. Soc.* **1938**, *60*, 309–319. [CrossRef]
37. Tauc, J.; Grigorovici, R.; Vancu, A. Optical Properties and Electronic Structure of Amorphous Germanium. *Phys. Status Solidi B* **1966**, *15*, 627–637. [CrossRef]
38. Taghizadeh, S.M.; Lal, N.; Ebrahiminezhad, A.; Moeini, F.; Seifan, M.; Ghasemi, Y.; Berenjian, A. Green and economic fabrication of zinc oxide (ZnO) nanorods as a broadband UV blocker and antimicrobial agent. *Nanomaterials* **2020**, *10*, 530. [CrossRef]
39. Rodríguez, C.; Tapia, C.; Leiva-Aravena, E.; Leiva, E. Graphene Oxide–ZnO Nanocomposites for Removal of Aluminum and Copper Ions from Acid Mine Drainage Wastewater. *Int. J. Environ. Res. Public Health* **2020**, *17*, 6911. [CrossRef]
40. Arias, M.; López, E.; Nuñez, A.; Rubinos, D.; Soto, B.; Barral, M.T.; Díaz-Fierros, F. Adsorption of methylene blue by red mud, an oxide-rich byproduct of bauxite refining. In *Effect of Mineral-Organic-Microorganism Interactions on Soil and Freshwater Environments*; Berthelin, J., Huang, P.M., Bollag, J.-M., Andreux, F., Eds.; Springer: Boston, MA, USA, 1999; pp. 361–365.
41. Yang, Y.; Guan, C. Adsorption properties of activated carbon fiber for highly effective removal of methyl orange dye. *IOP Conf. Ser. Earth Environ. Sci.* **2018**, *208*, 012005. [CrossRef]
42. Melián, E.P.; Díaz, O.G.; Rodríguez, J.D.; Colón, G.; Araña, J.; Melián, J.H.; Navío, J.A.; Peña, J.P. ZnO activation by using activated carbon as a support: Characterisation and photoreactivity. *Appl. Catal. A Gen.* **2009**, *364*, 174–181. [CrossRef]
43. Raizada, P.; Singh, P.; Kumar, A.; Sharma, G.; Pare, B.; Jonnalagadda, S.B.; Thakur, P. Solar photocatalytic activity of nano-ZnO supported on activated carbon or brick grain particles: Role of adsorption in dye degradation. *Appl. Catal. A Gen.* **2014**, *486*, 159–169. [CrossRef]
44. Byrappa, K.; Subramani, A.K.; Ananda, S.; Rai, K.L.; Sunitha, M.H.; Basavalingu, B.; Soga, K. Impregnation of ZnO onto activated carbon under hydrothermal conditions and its photocatalytic properties. *J. Mater. Sci.* **2006**, *41*, 1355–1362. [CrossRef]
45. Sobana, N.; Swaminathan, M. Combination effect of ZnO and activated carbon for solar assisted photocatalytic degradation of Direct Blue 53. *Sol. Energy Mater. Sol. Cells* **2007**, *91*, 727–734. [CrossRef]
46. Vinayagam, M.; Ramachandran, S.; Ramya, V.; Sivasamy, A. Photocatalytic degradation of orange G dye using ZnO/biomass activated carbon nanocomposite. *J. Environ. Chem. Eng.* **2018**, *6*, 3726–3734. [CrossRef]
47. Chen, G.; Wang, Y.; Dai, G.; Zhang, F. Immobilization of flower-like ZnO on activated carbon fibre as recycled photocatalysts. *Res. Chem. Intermed.* **2016**, *42*, 8227–8237. [CrossRef]
48. Abu-Dalo, M.A.; Nevostrueva, S.; Hernandez, M. Removal of radionuclides from acidic solution by activated carbon impregnated with methyl-and carboxy-benzotriazoles. *Sci. Rep.* **2020**, *10*, 1–13. [CrossRef]

49. Pathania, D.; Sharma, S.; Singh, P. Removal of methylene blue by adsorption onto activated carbon developed from Ficus carica bast. *Arab. J. Chem.* **2017**, *10*, 1445–1451. [CrossRef]
50. Pereira, M.F.R.; Soares, S.F.; Órfão, J.J.; Figueiredo, J.L. Adsorption of dyes on activated carbons: Influence of surface chemical groups. *Carbon* **2003**, *41*, 811–821. [CrossRef]
51. AL-Aoh, H.A.; Yahya, R.; Jamil Maah, M.; Radzi Bin Abas, M. Adsorption of methylene blue on activated carbon fiber prepared from coconut husk: Isotherm, kinetics and thermodynamics studies. *Desalin. Water Treat.* **2014**, *52*, 6720–6732. [CrossRef]
52. Yang, X.; Wang, D. Photocatalysis: From fundamental principles to materials and applications. *ACS Appl. Energy Mater.* **2018**, *1*, 6657–6693. [CrossRef]
53. Luo, S.; Liu, C.; Wan, Y.; Li, W.; Ma, C.; Liu, S.; Heeres, H.J.; Zheng, W.; Seshan, K.; He, S. Self-assembly of single-crystal ZnO nanorod arrays on flexible activated carbon fibers substrates and the superior photocatalytic degradation activity. *Appl. Surf. Sci.* **2020**, *513*, 145878. [CrossRef]
54. Shrestha, P.; Jha, M.K.; Ghimire, J.; Koirala, A.R.; Shrestha, R.M.; Sharma, R.K.; Pant, B.; Park, M.; Pant, H.R. Decoration of Zinc Oxide Nanorods into the Surface of Activated Carbon Obtained from Agricultural Waste for Effective Removal of Methylene Blue Dye. *Materials* **2020**, *13*, 5667. [CrossRef] [PubMed]